HOKKAIDO UNIVERSITY

Title	Analyses on the mechanism of a Convective Cloud System over the ishikari Plain on September 23, 1988
Author(s)	SHINODA, Taro; UYEDA, Hiroshi; YOSHIZAKI, Masanori
Citation	Journal of the Faculty of Science, Hokkaido University. Series 7, Geophysics, 11(1), 207-227
Issue Date	1998-03-20
Doc URL	http://hdl.handle.net/2115/8832
Type	bulletin (article)
File Information	11(1)_p207-227.pdf

Analyses on the Mechanism of a Convective Cloud System over the Ishikari Plain on September 23, 1988

Taro Shinoda, Hiroshi Uyeda

*Division of Earth and Planetary Sciences, Graduate School of Science,
Hokkaido University, Sapporo 060-0810, Japan*

and

Masanori Yoshizaki

*Meteorological Research Institute,
Tsukuba, Ibaraki 305-0052, Japan*

(Received November 30, 1997)

Abstract

Most severe storms that occur over the Ishikari Plain are concentrated in a specific area : the eastern suburb of Sapporo and the central area of the Ishikari Plain. To analyze the structure and mechanism of a convective cloud system which developed over the Ishikari Plain, Hokkaido, we investigated a severe storm which developed on September 23, 1988 using the results of the Doppler radar observation, ground and upper meteorological data, and three-dimensional numerical simulations using the moist cloud model developed by Yoshizaki and Ogura (1988). The results of the Doppler radar observation show that this convective cloud system propagated from the seaside area to the inland area over the Ishikari Plain. The convective cloud system was organized as a line oriented north-south propagating from the seaside area to the inland area. The orientation of the system upon reaching the inland area changed to southwest-northeast. From the results of the surface observations, a difference in the wind direction and speed near the ground between the seaside area and the inland area is considered in performing the numerical simulations and we obtained the results that this difference brought about the change in the orientation of the convective cloud system derived from the convergent area between the lower inflow (generally southerly or southeasterly wind) and the divergent flow from the system.

1. Introduction

Severe storms occur over the Ishikari Plain, Hokkaido, from May to October. Most of these storms occur in a specific area : the eastern suburb of Sapporo and the central area of the Ishikari Plain. There have been several investigations of these storms. Kobayashi and Kikuchi (1989) reported a

ground survey and radar analysis of a microburst event in Kita village, near Sapporo, on September 23, 1986. Kobayashi et al. (1996) investigated the life cycle of a tornado event in Chitose city, near Sapporo, on September 22, 1988. Takahashi et al. (1996) analyzed processes of the development of an isolated cloud formed in the south of Sapporo on July 9, 1992. However, these investigations did not refer to the mechanisms behind how these storms were generated and developed in the specific area.

There are two techniques to investigate the generation, development and dissipating processes of severe storms. One is by observation using a meteorological radar, surface observational networks and other measuring instruments. An advantage of this type of observation is that it gets successive and spatial data on actual phenomena, e.g. distributions of precipitation intensity and wind fields in severe storms. However, parameters to indicate the structure of the storm are restricted in the observation ; it is difficult to obtain pressure, temperature and water vapor fields. The other technique is a numerical simulation using a CRM (Cloud Resolution Model). An advantage of using the numerical simulation that it shows the most parameters to describe the cloud dynamics. Further, we can clarify what elements contribute to the mechanism of severe storms by adjusting the terms of governing equations to describe the numerical simulation.

Recently, many investigations comparing both of these techniques were performed. Klemp et al. (1981) and Wilhelmson and Klemp (1981) performed the analysis on supercell thunderstorms. Wilhelmson and Chen (1982) applied the above techniques on multicell thunderstorms. Ogura and Yoshizaki (1988) and Yoshizaki and Ogura (1988) included the effect of terrain on the CRM, showing that the terrain contributed to the development of the severe storm. However, no research has investigated what elements contribute to the mechanism of severe storms over the Ishikari Plain by using observational data and numerical simulation results at the same time.

On the afternoon of September 23, 1988, a severe storm developed in the central area of the Ishikari Plain and brought hailstones to Iwamizawa city. In this study, we will investigate the structure and mechanism of this severe storm using successive data obtained by a Doppler radar and surface meteorological observations. After detailed analyses, we will perform numerical simulations to illustrate the process of the generation and development of this storm. The purpose of this paper is to clarify what elements affected the development of this storm. Furthermore, we will compare results obtained by both observational data and numerical simulations.

2. Methods

2.1 Observation

Figure 1 shows a map of the topography around the Ishikari Plain, Hok-kaido.   The Ishikari Plain is bordered on the west, east and north by mountain areas, and faces the Sea of Japan to the northwest and the Pacific Ocean to the south.   The southern part of the Ishikari Plain forms as a valley extending from north to south whose width is about 40 km.

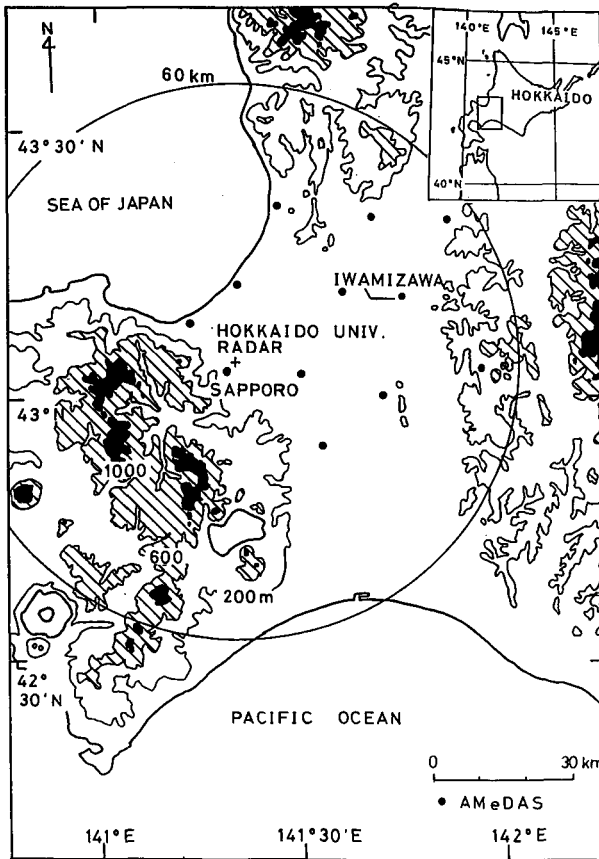The Doppler radar was set up in the Hokkaido University campus; its

Fig. 1. The topography around the Ishikari Plain, Hokkaido. Contour lines denote the height of 200, 600 and 1000 m, respectively. Hatched and solid areas denote higher than 600 m and 1000 m, respectively. The location of the radar site is depicted by a cross with a 60 km range circle. Solid circles show the positions of AMeDAS stations.

location is shown by a cross in Fig. 1. The radar collected the reflectivity, Doppler velocity and spectrum width of the Doppler velocity with a range resolution of 250 m in an observation range of 60 km. The wave length of this radar was 3.2 cm.

The observation was performed from 1350 to 1640 JST (9 hours ahead of UTC) at 10 minute intervals by 3 PPI scans and several RHI scans.

In this analysis the records of meteorological elements taken at Iwamizawa Weather Station and AMeDAS (Automated Meteorological Data Acquisition System) stations of Japan Meteorological Agency were used. Sounding data taken at Sapporo District Meteorological Observatory is used in the initial condition of the numerical simulations.

2.2 Model description

In this study a three-dimensional compressible moist cloud model developed by Yoshizaki and Ogura (1988) is used. The governing equations of this model include momentum, heat (potential temperature), mass (pressure), water substances, turbulent kinetic energy and the equation of state. These equations are represented in the Cartesian coordinate system, where x and y are the eastward and northward coordinate, respectively, and z is the vertical one.

In this study the warm rain microphysical parameterization of Kessler (1969) is also used, where water substances are divided into three forms : water vapor, cloud water and rain. Water substances of the ice phase are not included.

The boundary layer parameterization includes heat, water vapor and momentum flux from the surface. The open boundary conditions are used at the lateral boundaries. A sponge layer is included above the height of 13 km to prevent the reflection of internal gravity waves at the top boundary. The coefficient of Rayleigh friction in the sponge layer is assumed to be $0.001\,\mathrm{s}^{-1}$. The fourth order horizontal smoother is included to suppress the computational noise and the coefficient of the smoother is assumed to be $0.005\,\mathrm{s}^{-1}$. The model includes the Coriolis force and its parameter f is given as $9.95\times10^{-4}\,\mathrm{s}^{-1}$ (43°N).

The grid size in the x- and y-direction is constant and is taken to be 1.0 km, whereas the vertical grid size is stretched to allow a finer resolution in the lower atmosphere. The minimum vertical grid size is 120 m in the lowest layer and the middle level grid size is constant and taken to be 600 m. There are $120\times 120\times 35$ grid points in the x-, y- and z-direction, respectively, and the model domain is $120\times120\times20$ km.

Since storms would naturally move out of the modeled domain in the simulated time period, the coordinate system is translated at 5 m/s in the x-

direction and 3 m/s in the y-direction.

3. Meteorological conditions

The synoptic condition is shown in Fig. 2. The surface weather chart indicates that a high pressure system is located over the Pacific Ocean in the
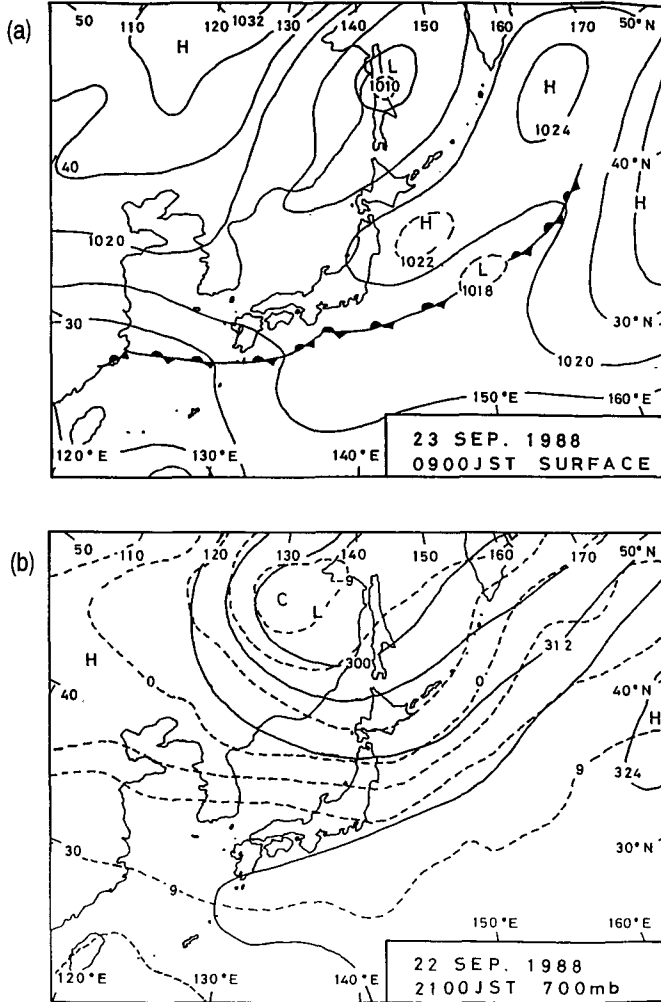

Fig. 2. (a) Surface weather chart at 0900 JST on September 23, 1988. The solid lines indicate the contours of isobar. (b) 700 mb weather chart at 2100 JST on September 22, 1988. The solid and dashed lines express the contours of geopotential height and isotherm, respectively.
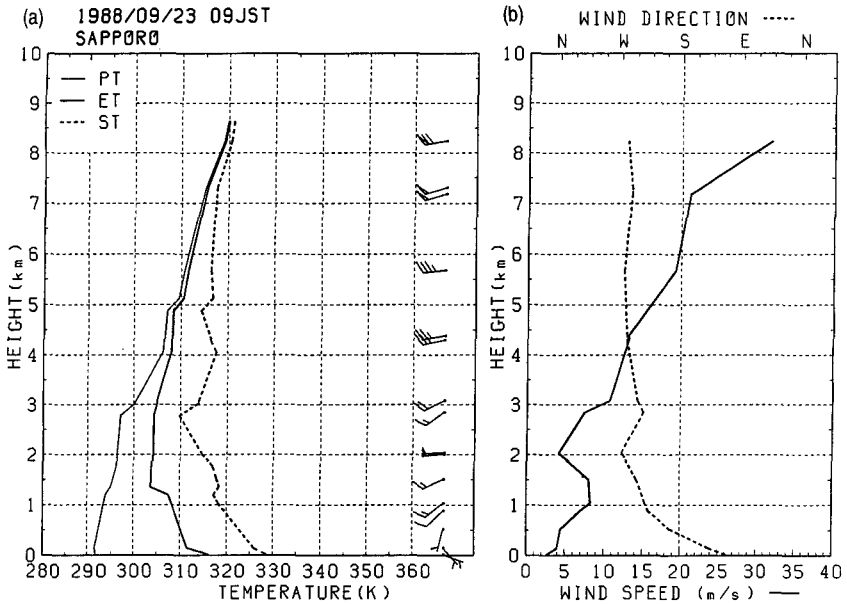
Fig. 3.   Vertical profiles of (a) potential temperature (PT), equivalent potential tem-
perature (ET) and saturated equivalent potential temperature (ST), and (b) wind
direction and wind speed at Sapporo at 0900 JST on September 23, 1988.

southeast of Hokkaido, and there is a low pressure system with a cold trough
located in the north of the Hokkaido.   Due to this condition, a warm southerly
advection occurred and an unstable condition prevailed in the observation area.
This synoptic pattern was quite similar to the Chitose tornado event on Septem-
ber 22, 1988 (Kobayashi et al., 1996) and other severe storm cases around the
Ishikari Plain.

Figure 3 presents the sounding data at 0900 JST at Sapporo.   The 0°C level
was located at an altitude of approximately 2.5 km.   The convective available
potential energy (CAPE) was 1153 m^2/s^2 computed from the soundings at 0900
JST at Sapporo.   The wind profile shows that the wind direction rotates
clockwise from southeast to west below 2.0 km and the westerly wind speed
increases along with the height above 2.0 km.

4.   Observational results

4.1   Doppler radar observational results

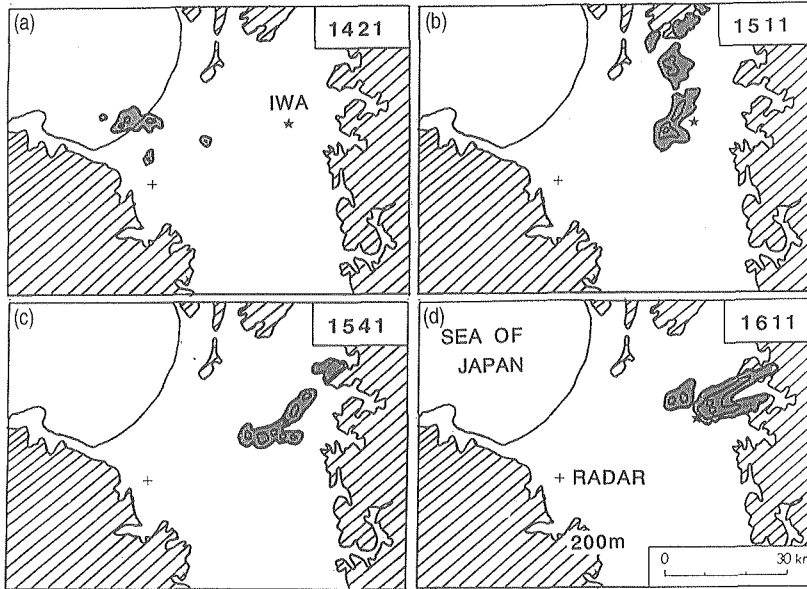The transition of the radar echoes on September 23, 1988, is represented in

Fig. 4. Reflectivity of the PPI scan (elevation angle is 3.0°) at (a) 1421, (b) 1511, (c) 1541
and (d) 1611 JST on September 23, 1988. Contour intervals are 6 dBZ from 21
dBZ. The hatched areas denote higher than 200 m. The location of the radar
site is depicted by a cross and the symbol (★) shows the position of Iwamizawa
Weather Station.

Fig. 4. The echoes propagate from the seaside area to the inland area over the
Ishikari Plain. At 1421 JST there is a convective cloud system consisting of
two echoes over the coastline of the Ishikari Bay. A vertical cross section of
this convective cloud system is shown in Fig. 5 four minutes the time of before
Fig. 4(a). In the Fig. 5(b) the positive and negative value denotes the wind speed
toward and away from the radar, respectively. A distinct divergent area exists
below the convective cell, therefore this was classified as being in a dissipating
stage of the life cycle of the convective cell. The divergence value estimated
from the Doppler velocity was of the order of 3×10^{-3} s^{-1}, if we assume that the
divergence was two dimensional. This divergence value was supported by 4
other vertical cross sections near the azimuth at this time.

Figure 6 presents the transition of reflectivity of the PPI scan at about 10
minute intervals. After 1421 JST, several convective echoes were generated,
developed and dissipated intermittently to maintain the convective cloud sys-
tem. The convective cloud system originated from the divergent flow observed
at 1421 JST. This divergent flow was brought from the first weak convective

RHI (330.0°)   23 SEP. 1988

(a)   1417 JST

REFLECTIVITY (dBZ)

(b)

DOPPLER VELOCITY (m/s)
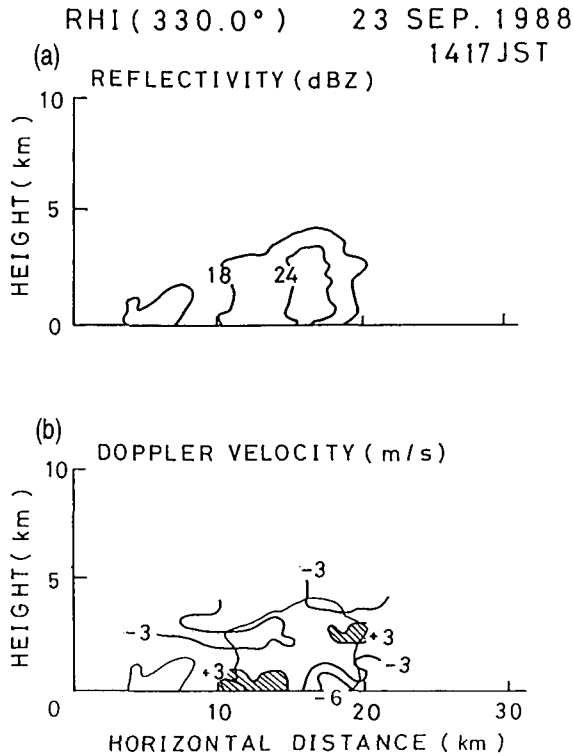

HORIZONTAL DISTANCE (km)

Fig. 5.   Vertical cross sections (RHI scan) of (a) reflectivity and (b) Doppler velocity
along 330.0° in azimuth at 1417 JST on September 23, 1988.   Contour intervals of
reflectivity are 6 dBZ from 18 dBZ and those of Doppler velocity are 3 m/s.

cells dissipating over the coastline of the Ishikari Bay as shown in Fig. 4(a) and
Fig. 5.   The convective cloud system was organized as a line oriented north-
south at 1511 JST shown in Fig. 4(b), when it propagated to the inland area.   In
this stage new convective echoes generated ahead of the old convective cloud
system.   Namely, the new echoes located to the east and oriented north-south
of the old system.

At 1541 JST the system changed its orientation from north-south to south-
west-northeast.   In this stage the new convective echoes were generated to the
right of the system propagation.   Namely, the new echoes located to the
southeast and oriented southwest-northeast of the old system.   This pattern
was quite similar to the typical multicell storms captured by Wilhelmson and
Chen (1982).

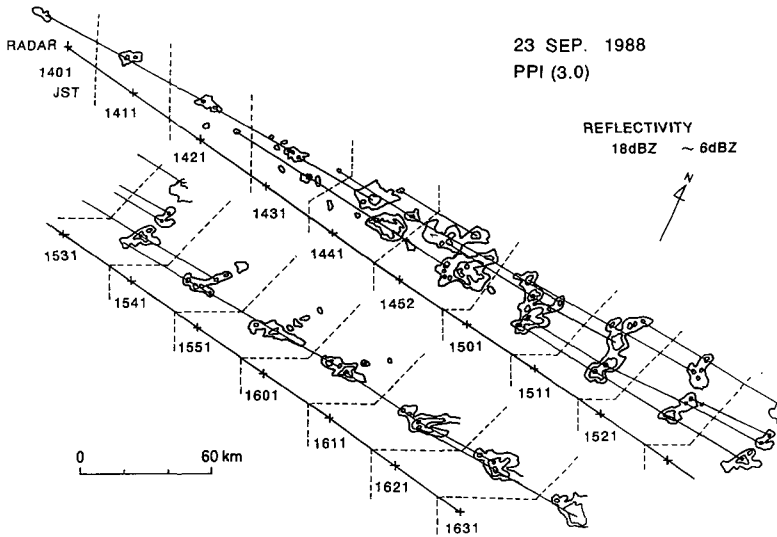Figure 7 shows vertical cross sections of the convective cloud system just

Fig. 6. Transition of reflectivity of the PPI scan (elevation angle is equal to 3.0°) from 1401 to 1631 JST on September 23, 1988. Contour intervals are 6 dBZ from 18 dBZ. A cross indicates the relative position of the radar site.

after a sudden change of meteorological elements at Iwamizawa Weather Station depicted in Fig. 10. The height of the echo top reaches 9 km and there is an area of large Doppler velocity away from the radar at the range of 42 km near the ground. It corresponded to the gust front observed at Iwamizawa Weather Station as described later.

4.2 Ground surface observational results

In the analytical region there are 12 AMeDAS stations and they obtain the records of meteorological elements at 10 minute intervals. The transition of the temperature at every AMeDAS station from 1000 to 1800 JST on September 23, 1988, is represented in Fig. 8. The temperature reaches 22-25°C at every station except YUB (Yubari) before noon by solar radiation. After 1400 JST there are significant temperature drops of about 3-7°C (depicted by solid wedges) e.g., ISK (Ishikari), SNT (Shin-Shinotsu) and IWA (Iwamizawa). The time that the temperature drops at the seaside area is earlier than that of the inland area. This situation coincided with the propagation of the convective cloud system. However, there is no phenomenon of the temperature drops in the southern area of the system, e.g., ENW (Eniwa-Shimamatsu) and NAG (Naganuma). These suggested the existence of a cold dome below the convective cloud system. It
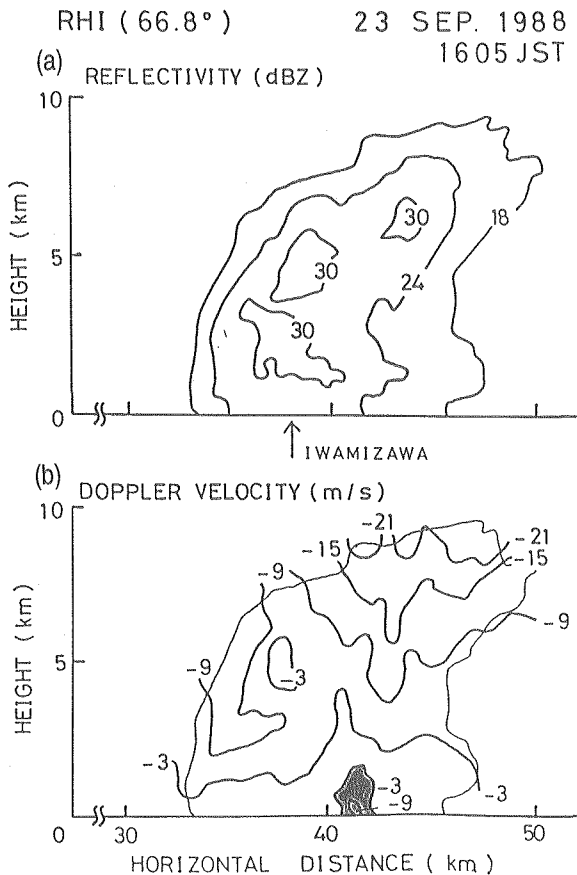
Fig. 7. Vertical cross sections (RHI scan) of (a) reflectivity and (b) Doppler velocity
along 66.9° in azimuth at 1605 JST on September 23, 1988. Contour intervals of
reflectivity are 6 dBZ from 18 dBZ and those of Doppler velocity are 3 m/s.
Iwamizawa Weather Station is located on this azimuth about 38 km far from the
radar site.

is generally explained that the cold dome is generated by the effect of the
evaporation cooling of precipitation particle below the cloud base of the
convective clouds.

Figure 9 shows the transition of the wind direction and speed as described
in Fig. 8. Before the passage of the convective cloud system, a remarkable
southeasterly wind of about 6-8 m/s is seen in the inland area of the Ishikari
Plain, while a weak easterly or southerly wind less than 4 m/s is seen in the
seaside area. Note that the seaside area has mountains to the south, whereas
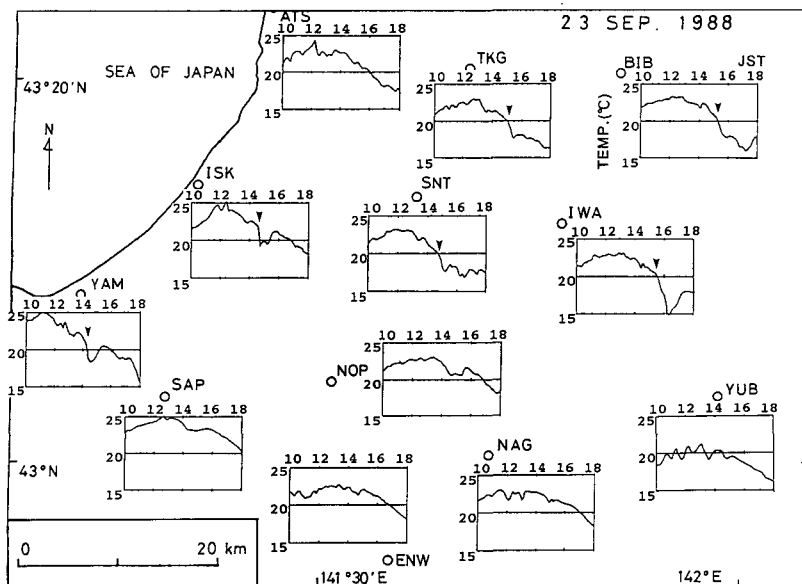
Fig. 8. Transition of the temperature at AMeDAS stations from 1000 to 1800 JST on September 23, 1988. Circles show the position of AMeDAS stations. The solid wedges depict the remarkable temperature drops.

the inland area does not have mountains to the south as shown in Fig. 1. It is considered that a lower wind was influenced by the surface morphology. Distinct changes in the wind direction near 1200 JST at YAM (Yamaguchi) and ISK (Ishikari), located near the coastline, corresponded to the intrusion of a sea breeze. The temperature drops associated with the intrusion of the sea breeze are seen at the same stations in Fig. 8. Two hours after the passage of the sea breeze, there are significant changes in wind direction (depicted by wedges) e.g., ISK (Ishikari), SNT (Shin-Shinotsu) and IWA (Iwamizawa). The time of these changes in wind direction correspond to that of the temperature drops. However, there are no changes in wind direction in the southern area of the system e.g., ENW (Eniwa-Shimamatsu) and NAG (Naganuma). This suggests the passage of a leading edge of an outflow from the convective cloud system.

    In order to investigate the characteristics of this leading edge, Fig. 10 shows the original records of meteorological elements at Iwamizawa Weather Station. A strong precipitation intensity of 13 mm per 10 minutes with hail, an abrupt change in wind direction from southeasterly or southerly to west-northwesterly, a peak of wind speed, and a significant temperature and dew point temperature drop are recognized. The changes of these meteorological elements corre-
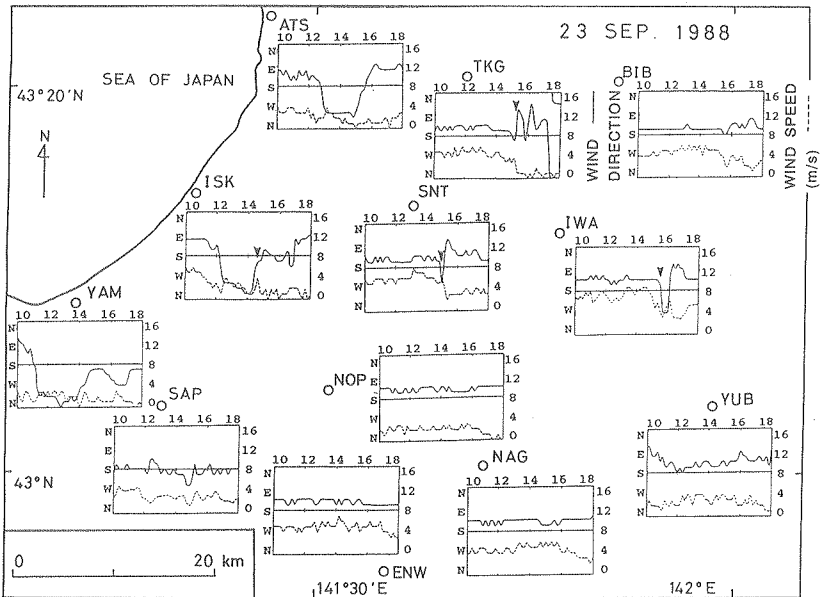
Fig. 9. Transition of the wind direction and speed at AMeDAS stations from 1000 to 1800 JST on September 23, 1988. Circles show the position of AMeDAS stations. The solid wedges depict the remarkable changes in the wind direction.

sponded to the passage of the gust front observed by the Doppler radar shown in Fig. 7. It is generally explained that this gust front was generated by the divergence of the downdraft from the convective cell near the ground.

5. Model results

5.1 Initialization

In the radar observation, a difference in the orientation of the convective cloud system was prominent; north-south during its propagation from the seaside area to the inland area and southwest-northeast after reaching to the inland. We supposed that the difference of the wind direction and speed near the ground caused the difference in the orientation of the convective cloud system. A remarkable southeasterly surface wind of about 6-8 m/s was seen in the inland area of the Ishikari Plain as shown in Fig. 9. However, the weak easterly or southerly surface wind less than 4 m/s was seen in the seaside area. The convective cloud system propagated from the weak easterly surface wind area to the strong southeasterly surface wind area. It was generally expected
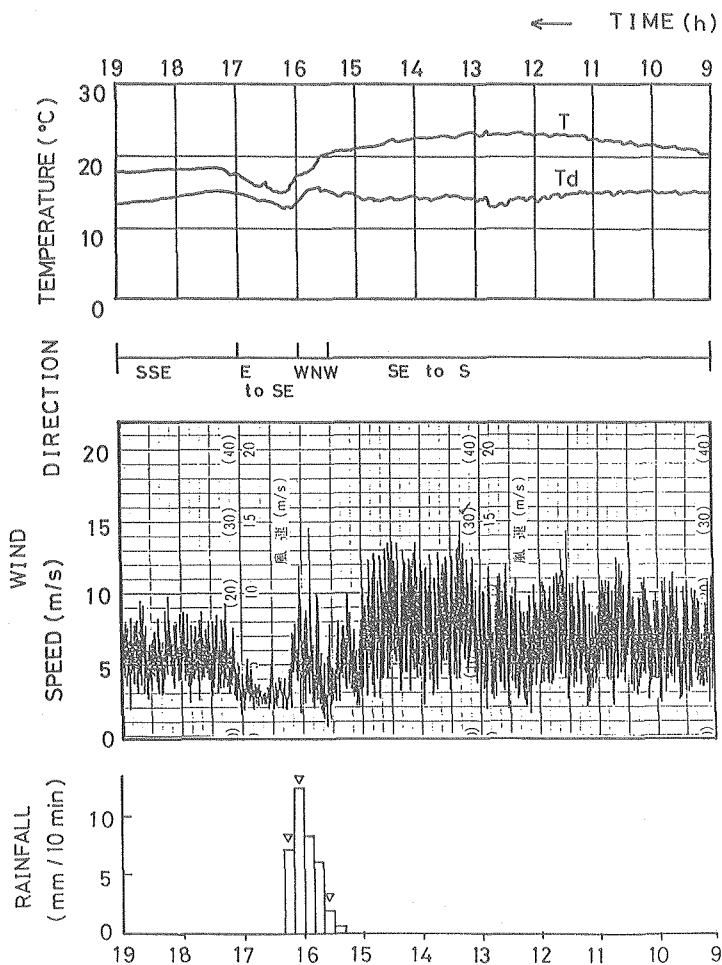
Fig. 10. Original records of temperature, dew point temperature, wind speed and
rainfall rate at Iwamizawa Weather Station from 0900 to 1900 JST on September
23, 1988.   The wind direction data is displayed at Iwamizawa AMeDAS station
because of no observational data exists at Iwamizawa Weather Station at this
time.   The wedges depict the hailstone observed at this point.

that the effect of the surface wind reached the top of the planetary boundary
layer.   We performed three dimensional numerical simulations to confirm the
effect of the strong southerly wind in the planetary boundary layer to generate
the convective cloud system.

The initial basic states in the simulations were the soundings at 0900 JST at Sapporo with some modifications. One modification was the thermodynamic condition in the lower layer. We adopted the isentropic atmosphere below 900 hPa to consider the effect of the growth of the mixing layer by the solar radiation. The temperature at the surface was 24°C. After this modification the CAPE was about 2500 m²/s². The other modification was the wind direction and speed near the ground. For the period of the convective cloud system propagation to the inland area (stage A), the sounding at 0900 JST at Sapporo was used without modification, because the surface wind direction (110°) and speed (2.7 m/s) of the sounding was quite similar to that of AMeDAS in the seaside area e.g., ISK (Ishikari). For the period after the convective cloud system reaching to the inland area (stage B), the wind direction and speed below 900 hPa was adopted at 150° and 10 m/s, respectively, and the values from 900 hPa to 850 hPa were interpolated linearly.

A thermal was placed on the center of the model domain to trigger the convective cloud system. The thermal was oblate with a horizontal axis of 3 km and a vertical axis of 750 m was placed at the height of 1250 m. The thermal had a maximum magnitude of 5 K at the center, decreasing to 0 K at the edges. It is assumed that relative humidity was 100% and no cloud water existed in the initial thermal.

It is generally explained that a convective cell generated by the initial thermal produces a downdraft in the mid-level of the cell after its mature stage ; the downdraft is induced by the drag forcing of precipitation droplets and evaporation cooling of rainwater. The downdraft from the convective cell diverges and generates a gust front near the ground. This gust front produces a convergent area with a general wind near the ground and new convective cells are generated at that area. This process occurs repeatedly and a convective cloud system is maintained in the numerical simulation in this manner.

5.2 Stage A

First, the typical result from stage A is shown. It is seen in Fig. 11 that a distinct downdraft area at the height of 1 km corresponds to a divergent area at the surface. Simultaneously, there are updraft areas at the height of 2 km which are induced by the convergence between the gust front from the old dissipating convective cell and the general easterly wind near the surface. Note that these convective cells form a line oriented north-south.

In Fig. 12 the left of convective cells has a downdraft, and a negative temperature anomaly expands horizontally below the cell. Therefore, this is
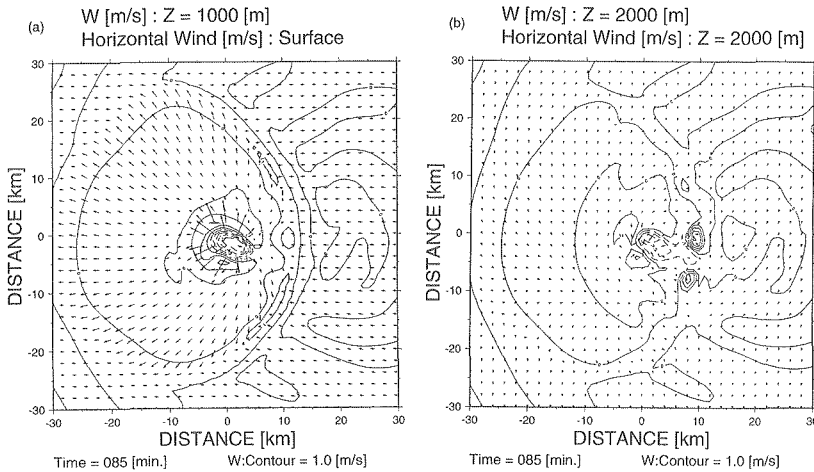
Fig. 11. (a) Horizontal wind vectors at the surface and vertical wind speed on the
height of 1.0 km, (b) horizontal wind vectors and vertical wind speed on the height
of 2.0 km at 85 minutes after the model initialization in the model for the stage A.
The solid and dashed lines express the contours of updraft and downdraft wind
speed, respectively and the contour interval is 1.0 m/s.

classified as being in a dissipating stage of a life cycle of the convective cell,
whereas the right has an updraft and a warm core. In this area the condensa-
tion of water vapors proceeds and the latent heat of condensation is released,
then the temperature anomaly and cloud mixing ratio (liquid water content) are
positive. Therefore, this convective cell corresponds to a developing stage of
the life cycle and is maintained by a easterly inflow. As the convergence is
weak, the new convective cell does not develop actively and the cloud top is
about 4 km. The echo top of this stage observed by the Doppler radar is about
9 km (not shown). Thus, the cloud top in the model is estimated lower than the
observational results.

5.3 Stage B

Next, the typical result from stage B is shown. It is seen in Fig. 13 that a
distinct downdraft area at the height of 1 km corresponds to a divergent area at
the surface. An updraft area is generated around the south and east sides of the
downdraft area. The shape of the updraft area forms an arc oriented south-
west-northeast and is different from that of stage A. Namely, the new updraft
area is induced by the convergence between the gust front from the old dissipat-
ing convective cell and the generally strong southeasterly wind near the surface.

In Fig. 14 there are two convective cells as shown in Fig. 12. The right of
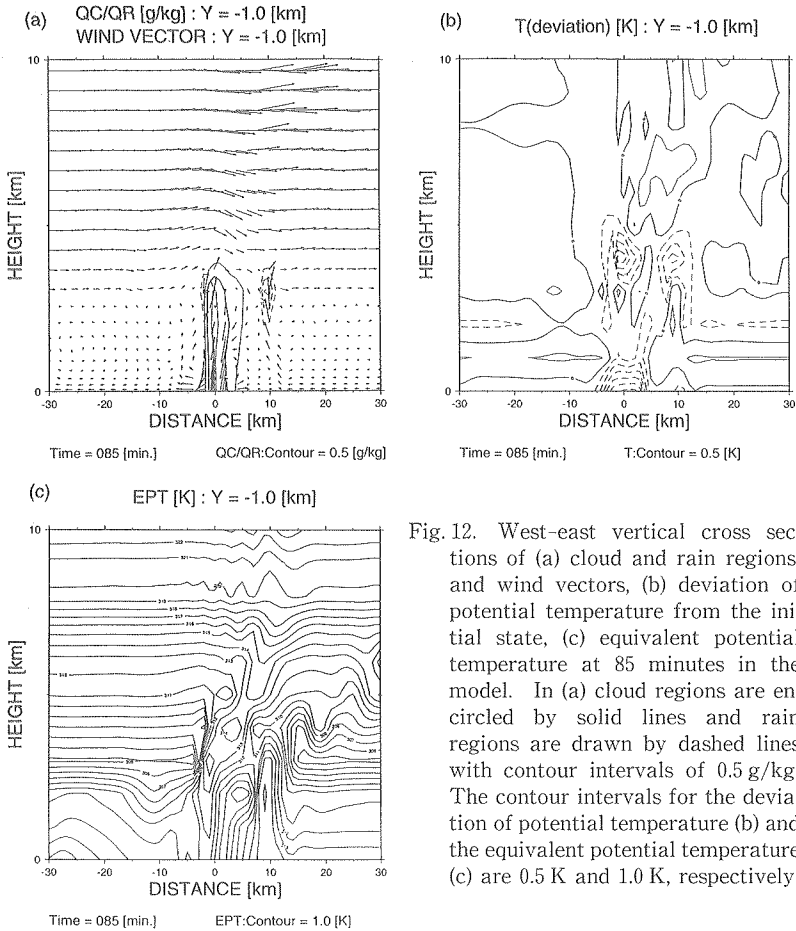
(a)   QC/QR [g/kg] : Y = -1.0 [km]
      WIND VECTOR : Y = -1.0 [km]

Time = 085 [min.]   QC/QR:Contour = 0.5 [g/kg]

(b)   T(deviation) [K] : Y = -1.0 [km]

Time = 085 [min.]   T:Contour = 0.5 [K]

(c)   EPT [K] : Y = -1.0 [km]

Time = 085 [min.]   EPT:Contour = 1.0 [K]

Fig. 12. West-east vertical cross sec-
          tions of (a) cloud and rain regions,
          and wind vectors, (b) deviation of
          potential temperature from the ini-
          tial state, (c) equivalent potential
          temperature at 85 minutes in the
          model. In (a) cloud regions are en-
          circled by solid lines and rain
          regions are drawn by dashed lines
          with contour intervals of 0.5 g/kg.
          The contour intervals for the devia-
          tion of potential temperature (b) and
          the equivalent potential temperature
          (c) are 0.5 K and 1.0 K, respectively.

convective cells (northern side) has a downdraft and a negative temperature
anomaly expands horizontally below the cell, therefore this is classified as being
in a dissipating stage of the life cycle of the convective cell.   Whereas, the left
(southern side) has an updraft and a warm core, therefore the left is classified as
being in a developing stage of the life cycle and is maintained by a southeasterly
inflow shown in Fig. 13.   In this simulation the cloud top is about 4 km which is
less than the observational results shown in Fig. 7.   This underestimation of the
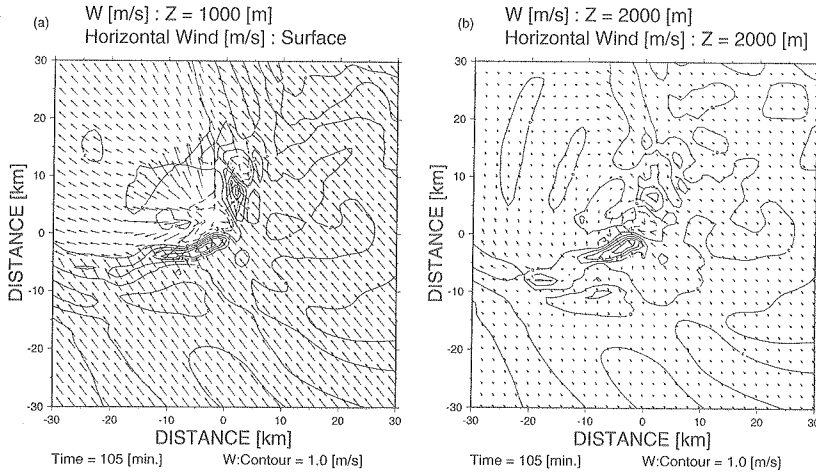height of the cloud tops is the same as that of stage A.

Fig. 13.   As in Fig. 11, except at 105 minutes for the stage B.

6.   Discussion

We discuss details of the differences between the observational results and the numerical simulation results in each stage of development of the convective cloud system.   The first stage is the initial dissipating cell over the coastline of the Ishikari Bay.   In this stage a distinct divergent area existed below the convective cell from the Doppler radar observation, and significant temperature drops and changes in wind direction were observed at AMeDAS stations near the seaside area.   In the numerical simulations these corresponded to the dissipation of the convective cell generated by the initial thermal ; a divergent area and a cold dome existed below the convective cell.   The methods of initialization with a thermal have been used frequently in other investigations, but there are several unanswered questions surrounding what causes the bubble in actual phenomena.   We propose that one of these causes is the effect of a gravity wave derived from another convection, another proposed cause is a large scale convergence such as regional fronts or cold fronts on a synoptic scale.   This is the subject for future study.

The second stage is the convective cloud system propagating from the seaside area to the inland area and this corresponds to stage A.   In this stage the convective cloud system was organized as a line oriented north-south from the results of the Doppler radar observation.   These Doppler radar observation results corresponded to the results of the numerical simulation for this stage. The numerical simulation showed that newly generated convective cells were
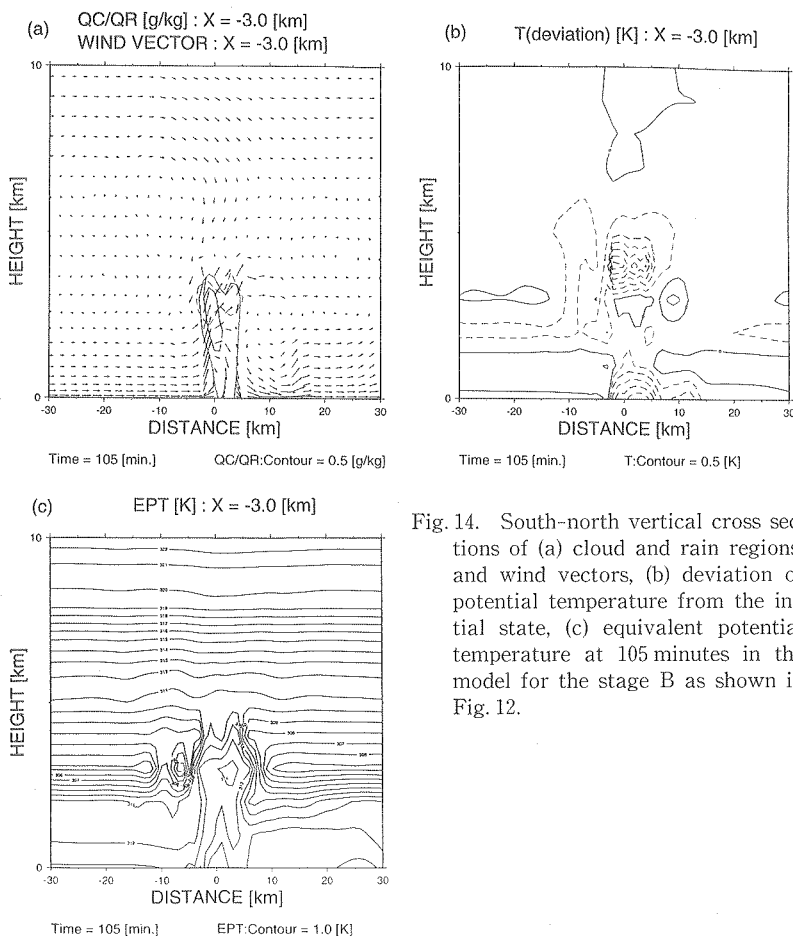
(a) QC/QR [g/kg] : X = -3.0 [km]
    WIND VECTOR : X = -3.0 [km]

(b)   T(deviation) [K] : X = -3.0 [km]

Time = 105 [min.]   QC/QR:Contour = 0.5 [g/kg]

Time = 105 [min.]   T:Contour = 0.5 [K]

(c)   EPT [K] : X = -3.0 [km]

Fig. 14. South–north vertical cross sec-
tions of (a) cloud and rain regions,
and wind vectors, (b) deviation of
potential temperature from the ini-
tial state, (c) equivalent potential
temperature at 105 minutes in the
model for the stage B as shown in
Fig. 12.

Time = 105 [min.]   EPT:Contour = 1.0 [K]

organized as a line oriented north–south, because a convergent area between a
easterly inflow and a divergent flow of the convective cloud system was generat-
ed around the east side of the system.   Significant temperature drops were
observed with the passage of the convective cloud system at AMeDAS stations
located in the central area of the Ishikari Plain.   A divergent area and a cold
dome existed below the convective cloud system and the new cell was
maintained by the convergence in the numerical simulation.

      The third stage is the convective cloud system reaching to the inland area
and this corresponds to stage B.   In this stage the convective cloud system was
organized as a line oriented southwest–northeast as shown in the results of the
Doppler radar observation.   In the numerical simulation for this stage these

Doppler radar observation results corresponded with the results that newly generated convective cells were organized as an arc oriented southwest-northeast, because a convergent area between a southeasterly inflow and a divergent flow of the convective cloud system was generated around the southeast side of the system.   Significant temperature drops, wind direction changes, passage of a gust front and hail precipitation were observed with the passage of the convective cloud system at Iwamizawa Weather Station.   A divergent area and a cold dome existed below the convective cloud system and the new cells were maintained by the convergence in the numerical simulation.

In these simulations we could not simulate the height of the cloud top of the convective system.   The height of the echo top obtained by the Doppler radar was about 9 km.   The height of the cloud top computed from the sounding used in the numerical simulations was about 8 km.   However, the height of the cloud top derived from these numerical simulations were about 5 km, which was lower than the height obtained from the observations.   We could attribute this discrepancy to the exception of the ice phase in the microphysical processes.   If we had included the ice phase in the numerical simulations, it is expected that a release of latent heat due to the freezing of cloud and rain water would develop the convection more actively and the cloud top would become higher than seen in these results.   Therefore, the inclusion of the ice phase in the CRM is the subject for future study.

Furthermore, the difference in the wind direction and speed near the ground between the seaside area and the inland area is considered in performing the numerical simulations and would be influenced by the surface morphology ; the distribution of mountains and coastlines.   The southern part of the Ishikari Plain is bordered on the west and east by mountain areas which forms a valley. Therefore, a distinguished lower southerly wind blown over the Ishikari Plain is accelerated by the convergence induced by the terrain.   A convergence between this strengthened lower southerly wind and local northerly wind ; a thunderstorm outflow or a sea breeze from the Sea of Japan, is possible to generate the convective cloud system over the specific area.   It is necessary to perform the numerical simulations included the actual terrain.

7. Conclusions

The structure and mechanism of the convective cloud system over the Ishikari Plain, on September 23, 1988 was revealed from the results of the Doppler radar observation, ground and upper meteorological data, and three-
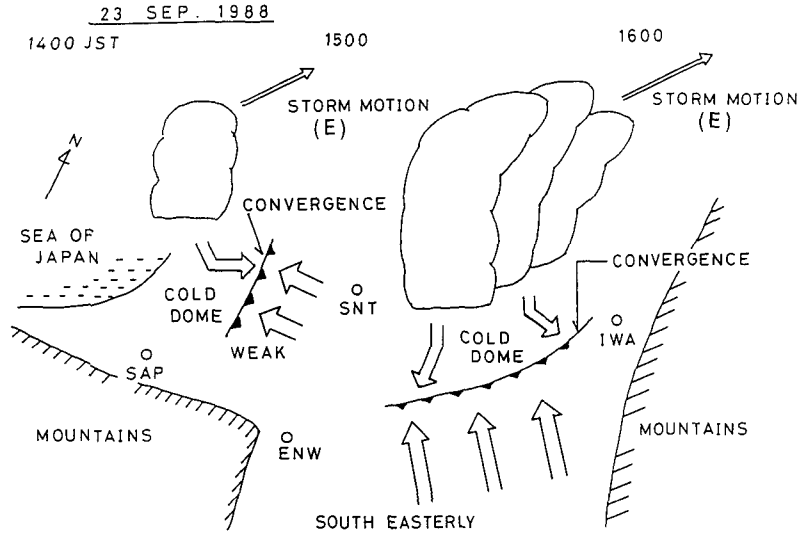
Fig. 15. Conceptual models of convective cloud system developed over the Ishikari
   Plain on September 23, 1988.

dimensional numerical simulations using the moist cloud model developed by
Yoshizaki and Ogura (1988). The conceptual model of the convective cloud
system obtained from this investigation is shown in Fig. 15. This convective
cloud system propagated from the seaside area to the inland area over the
Ishikari Plain. This system originated from the divergent flow brought from
the downdraft in the dissipating cell over the coastline of the Ishikari Bay. The
convective cloud system was organized as a line oriented north-south with
propagating from the seaside area to the inland area. In this stage the lower
easterly or southerly wind was weak, whereas the orientation of the system
reaching to the inland area changed to southwest-northeast. In this stage the
remarkable lower southeasterly wind was seen in the inland area of the Ishikari
Plain. Therefore, the difference in the wind direction and speed near the
ground between the seaside area and the inland area is considered in performing
the numerical simulations and we obtained the results that this difference
brought about the change in the orientation of the convective cloud system
which was derived from the convergent area between the lower inflow (generally
southerly or southeasterly wind) and the divergent flow of the system.

Acknowledgments

References

Kessler, E., 1969. On the distribution and continuity of water substance in atmospheric circulation. Meteor. Monogr., Amer. Meteor. Soc., **10**, 84 pp.

Klemp, J.B., R.B. Wilhelmson and P.S. Ray, 1981. Observed and numerically simulated structure of a mature supercell thunderstorm. J. Atmos. Sci., **38**, 1558-1580.

Kobayashi, F. and K. Kikuchi, 1989. A microburst phenomenon in Kita village, Hokkaido on September 23, 1986. J. Meteor. Soc. Japan, **67**, 925-936.

Kobayashi, F., K. Kikuchi and H. Uyeda, 1996. Life cycle of the Chitose tornado of September 22, 1988. J. Meteor. Soc. Japan, **74**, 125-140.

Ogura, Y. and M. Yoshizaki, 1988. Numerical study of orographic-convective precipitation over the Eastern Arabian Sea and the Ghat Mountains during the summer monsoon. J. Atmos. Sci., **45**, 2097-2122.

Takahashi, N., H. Uyeda and K. Kikuchi, 1996. Evolution process and precipitation particles of an isolated echo observed with dual-polarization Doppler radar near Sapporo on July 9, 1992. J. Fac. Sci., Hokkaido Univ., Ser. VII (Geophysics), **10**, 135-153.

Wilhelmson, R.B. and J.B. Klemp, 1981. A three-dimensional numerical simulation of splitting severe storms on 3 April 1964. J. Atmos. Sci., **38**, 1581-1600.

Wilhelmson, R.B. and C.S. Chen, 1982. A simulation of development successive cells along a cold outflow boundary. J. Atmos. Sci., **39**, 1466-1483.

Yoshizaki, M. and Y. Ogura, 1988. Two- and three-dimensional modeling studies of the Big Thompson storm. J. Atmos. Sci., **45**, 3700-3722.